

A comparison of shrinkage estimators of the cosmological precision matrix

Marnix J. Looijmans,   Mike (Shengbo) Wang  and Florian Beutler 

¹Institute for Astronomy, University of Edinburgh, Royal Observatory Edinburgh, Blackford Hill, Edinburgh EH9 3HJ, UK

Accepted XXX. Received YYY; in original form 21 February 2024

ABSTRACT

The determination of the covariance matrix and its inverse, the *precision* matrix, is critical in the statistical analysis of cosmological measurements. The covariance matrix is typically estimated with a limited number of simulations at great computational cost before inversion into the precision matrix; therefore, it can be ill-conditioned and overly noisy when the sample size n used for estimation is not much larger than the data vector dimension. In this work, we consider a class of methods known as *shrinkage* estimation for the precision matrix, which combines an empirical estimate with a target that is either analytical or stochastic. These methods include linear and non-linear shrinkage applied to the covariance matrix (the latter represented by the so-called NERCOME estimator), and the direct linear shrinkage estimation of the precision matrix which we introduce in a cosmological setting. Using Bayesian parameter inference as well as metrics like matrix loss functions and the eigenvalue spectrum, we compare their performance against the standard sample estimator with varying sample size n . We have found the shrinkage estimators to significantly improve the posterior distribution at low n , especially for the linear shrinkage estimators either inverted from the covariance matrix or applied directly to the precision matrix, with an empirical target constructed from the sample estimate. Our results should be particularly relevant to the analyses of Stage-IV spectroscopic galaxy surveys such as the Dark Energy Spectroscopic Instrument (DESI) and *Euclid*, whose statistical power can be limited by the computational cost of obtaining an accurate precision matrix estimate.

Key words: methods: statistical – methods: data analysis – methods: numerical – large-scale structure of the Universe

1 INTRODUCTION

With the arrival of Stage-IV spectroscopic galaxy surveys such as the Dark Energy Spectroscopic Instrument (DESI)¹ (DESI Collaboration 2024, 2023) and *Euclid*² (Laureijs et al. 2011), we will be able to observe cosmic structure on scales larger than ever before. At the same time, there has been significant development in perturbative models of non-linear clustering on smaller scales (e.g. Perko et al. 2016; d’Amico et al. 2020; Semenaitė et al. 2022). The wider dynamic range accessible to galaxy surveys poses a statistical challenge as the number of modes of cosmological fluctuations becomes very large, especially for the determination of the associated covariance matrix that is vital to most data analyses.

The covariance matrix characterizes the uncertainties and thus the constraining power of the analysis. Whilst it is sometimes possible to derive an analytical expression from perturbation theory (e.g. Grieb et al. 2016; Li et al. 2019; Sugiyama et al. 2020; Wadekar et al. 2020), including higher-order corrections and accounting for systematic effects such as the survey window is far from straightforward (Wadekar & Scoccimarro 2020). The alternative is an empirical approach whereby a sample estimate of the covariance matrix is obtained from a limited number of high-fidelity mock realizations. The main challenge with this method is that the number of realizations depends

on the dimension of the data vector, which can mean that thousands of mock catalogues are needed. Because the evaluation of the likelihood function typically requires the inversion of the covariance matrix into the precision matrix, the covariance matrix estimate must not be singular, which is the case when the number of realizations is no greater than the data vector dimension. Previous studies (Taylor et al. 2013; Taylor & Joachimi 2014; Sellentin & Heavens 2016) have also shown that using only a limited number of data realizations to estimate the covariance matrix induces noise to which the operation of matrix inversion is highly sensitive. Moreover, since matrix inversion is a non-linear operation, an unbiased estimator of the covariance matrix does not generally result in an unbiased estimator of the precision matrix (Hartlap et al. 2006).

To alleviate the issues associated with covariance matrix estimation, resampling methods such as jackknife and bootstrapping have been proposed (e.g. Friedrich et al. 2015; Escoffier et al. 2016; O’Connell & Eisenstein 2019; Philcox et al. 2019; Mohammad & Percival 2022), which construct the covariance matrix from sub-samples of the observed data itself. However, these sub-samples are obtained by dividing the original simulations into much smaller sub-volumes, which do not necessarily contain the largest modes of interest.

In this work, we investigate an alternative class of methods known as *shrinkage* estimation, which combines empirical estimates of the covariance matrix with a *target* that is often (but not always) an analytical proxy. The standard linear shrinkage method in the statistical literature (Ledoit & Wolf 2003, 2004; Schäfer & Strimmer 2005) has been previously explored in a cosmological context by Pope

* Email: M.J.Looijmans@sms.ed.ac.uk

¹ desi.lbl.gov

² sci.esa.int/euclid, euclid-ec.org

Table 1. Notation used in this work.

Symbol	Definition
$\text{diag } \mathbf{A}$	Diagonal matrix consisting of the diagonal elements of \mathbf{A}
$\ \mathbf{A}\ _{\text{F}}$	Frobenius norm given by $[\text{tr}(\mathbf{A}\mathbf{A}^{\top})]^{1/2}$
$\ \mathbf{A}\ _{\text{tr}}$	Trace norm given by $\text{tr}[(\mathbf{A}\mathbf{A}^{\top})^{1/2}]$
$\llbracket a, b \rrbracket$	Closed integer interval
d	Length of the data vector
n	Number of data realizations
p	Number of inferred parameters
$\mathbf{X} \in \mathbb{R}^{d \times n}$	Data matrix
$\Sigma \in \mathbb{R}^{d \times d}$	True covariance matrix
$\Psi \in \mathbb{R}^{d \times d}$	True precision matrix given by Σ^{-1}
\mathbf{S}	Sample estimator of Σ
$\mathbf{\Pi}$	Sample estimator of Ψ
\mathbf{T}	Covariance matrix target
$\mathbf{\Pi}_0$	Precision matrix target
$\hat{\Sigma}_{\text{LS}}$	Linear shrinkage estimator of Σ
$\hat{\Psi}_{\text{LS}}$	$\hat{\Sigma}_{\text{LS}}^{-1}$, inverted covariance shrinkage estimator of Ψ
$\hat{\Sigma}_{\text{NLS}}$	Non-linear shrinkage (NERCOME) estimator of Σ
$\hat{\Psi}_{\text{NLS}}$	$\hat{\Sigma}_{\text{NLS}}^{-1}$, NERCOME estimator of Ψ
$\mathbf{\Pi}_{\text{LS}}$	Direct linear shrinkage estimator of Ψ
λ	Linear-shrinkage intensity parameter
α, β	Linear-shrinkage mixing parameters
s	NERCOME split parameter

& Szapudi (2008), and the NERCOME³ estimator from non-linear shrinkage methods (Ledoit & Wolf 2012) has been first introduced by Joachimi (2017) in the same context. In both methods, the shrinkage estimate of the covariance matrix still needs to be inverted into the precision matrix estimate for likelihood analysis, and the effect of inversion is not yet fully understood. We will compare the performance of these two estimation methods with a third method, introduced and applied here in a cosmological context for the first time, which applies linear shrinkage directly to precision matrix estimation instead (Bodnar et al. 2016).

This paper is organized as follows: we introduce the different covariance and precision matrix estimators in section 2, and apply them to a power spectrum analysis in section 3; we then compare their performance in section 4, and discuss our findings before concluding in section 5.

For reference and clarity, our notation is listed in Table 1. For reproducibility and reference, the implementation of the different estimation methods considered in this work can be found in our public repository online (see Data Availability for details).

2 ESTIMATION METHODS

In this section, we describe the different precision matrix estimation methods to be compared. Most of them invert a covariance matrix estimate at the final stage, but the new method we adopt involves matrix inversion only as an intermediate step. The implications of covariance matrix inversion will be discussed.

³ Non-parametric Eigenvalue-Regularized COvariance Matrix Estimator

2.1 Sample estimation

Suppose we have a data matrix $\mathbf{X} \in \mathbb{R}^{d \times n}$ consisting of n independent realizations of a random vector of length d , which has an underlying covariance matrix $\Sigma \in \mathbb{R}^{d \times d}$ that is a priori unknown. Without loss of generality, we assume the data vectors are mean-subtracted. The standard sample estimator of the covariance matrix is then given by

$$\mathbf{S} = \frac{1}{n-1} \mathbf{X} \mathbf{X}^{\top}. \quad (1)$$

It is unbiased with expectation $\mathbb{E}[\mathbf{S}] = \Sigma$.

In a typical likelihood function, it is the precision matrix that appears instead of the covariance matrix, so one may wish to estimate the true precision matrix $\Psi \equiv \Sigma^{-1}$. From equation (1), we obtain the sample precision matrix estimator

$$\mathbf{\Pi} = \gamma \mathbf{S}^{-1}, \quad (2)$$

where the prefactor

$$\gamma = \frac{n-d-2}{n-1} \quad (3)$$

corrects for the multiplicative bias resulting from the inversion of the covariance matrix estimator \mathbf{S} , which is a non-linear operation. This prefactor γ is commonly known as the ‘Hartlap factor’ in cosmological analyses (Hartlap et al. 2006). It is immediately clear that the number of data realizations must satisfy $n > d+2$, and in the limit $n \rightarrow \infty$, \mathbf{S}^{-1} represents an asymptotically unbiased precision matrix estimator in itself.

2.2 Linear shrinkage

The *linear shrinkage* (LS) method uses a convex combination of an empirical covariance matrix estimate $\hat{\Sigma}$ and a *target* matrix \mathbf{T} to construct a new covariance matrix estimator (Ledoit & Wolf 2003, 2004),

$$\hat{\Sigma}_{\text{LS}} = (1-\lambda)\hat{\Sigma} + \lambda\mathbf{T}, \quad (4)$$

where $\lambda \in [0, 1]$ is the shrinkage *intensity*. The empirical estimate $\hat{\Sigma}$ is commonly chosen to be the *unbiased* sample covariance matrix estimate \mathbf{S} in equation (1), which we shall assume for the rest of this work; the target \mathbf{T} is often, but not always, an analytical quantity.

The idea behind shrinkage methods is that the target matrix has a smaller variance (possibly zero) than the empirical estimate, but may be otherwise biased, and one aims to find the optimal trade-off between bias and variance. Following Pope & Szapudi (2008), we first define

$$\bar{W}_{ij} = \frac{1}{n} \sum_{k=1}^n W_{ij}^{(k)} \quad \text{with} \quad W_{ij}^{(k)} = x_i^{(k)} x_j^{(k)}, \quad (5)$$

where $x_i^{(k)}$ is the (i, k) -th element of \mathbf{X} . The elements of the sample covariance matrix are then given by

$$S_{ij} = \frac{n}{n-1} \bar{W}_{ij}, \quad (6)$$

whose covariance can be estimated by

$$\widehat{\text{Cov}}(S_{ij}, S_{lm}) = \frac{n}{(n-1)^3} \sum_{k=1}^n (W_{ij}^{(k)} - \bar{W}_{ij})(W_{lm}^{(k)} - \bar{W}_{lm}). \quad (7)$$

Ledoit & Wolf (2003) and Schäfer & Strimmer (2005) have shown that the optimal intensity parameter is estimated by

$$\hat{\lambda}^* = \frac{\sum_{i,j} [\widehat{\text{Var}}(S_{ij}) - \widehat{\text{Cov}}(S_{ij}, T_{ij})]}{\sum_{i,j} (S_{ij} - T_{ij})^2}, \quad (8)$$

where $\widehat{\text{Var}}(S_{ij}) \equiv \widehat{\text{Cov}}(S_{ij}, S_{ij})$. If $\hat{\lambda}^*$ is found to be negative, it is then clipped to $\hat{\lambda}^* = 0$; if it is greater than 1, it is clipped to $\hat{\lambda}^* = 1$.

Finally, an estimate of the precision matrix is obtained by inversion, $\hat{\Psi}_{\text{LS}} = \hat{\Sigma}_{\text{LS}}^{-1}$. Since there is no general analytical form for the probability distribution of $\hat{\Sigma}_{\text{LS}}$, unlike for the sample estimator \mathbf{S} which follows the Wishart distribution (Hartlap et al. 2006), we do not include an analogous Hartlap factor here (de la Torre et al. 2013).

2.3 Non-linear shrinkage

The linear shrinkage estimator is in fact a first-order approximation to a more general class of *non-linear shrinkage* (NLS) estimators that attempt to shrink the dynamic range of the eigenvalues of the covariance matrix estimate and thus mitigate ill-conditioning when the data vector dimension becomes large (Ledoit & Wolf 2012). In this work, we consider in particular the *NERCOME estimator* of the covariance matrix proposed by Ledoit & Wolf (2012), Abadir et al. (2014) and Lam (2016), which has been previously applied by Joachimi (2017) and Gouyou Beauchamps et al. (2023) in a cosmological setting.

The NERCOME estimator is constructed from a set of data realizations as follows:

- (i) Without necessarily preserving their order, the columns of the data matrix \mathbf{X} are split into a $d \times s$ matrix \mathbf{X}_1 and a $d \times (n - s)$ matrix \mathbf{X}_2 for a given value of the split parameter $s \in \llbracket 2, n - 2 \rrbracket$;
- (ii) Two sample estimates of the covariance matrix, denoted \mathbf{S}_1 and \mathbf{S}_2 , are obtained from \mathbf{X}_1 and \mathbf{X}_2 respectively;
- (iii) The sample estimates are diagonalized, $\mathbf{S}_a = \mathbf{U}_a \mathbf{D}_a \mathbf{U}_a^\top$ with $a \in \{1, 2\}$, where \mathbf{D}_a is the diagonal matrix of eigenvalues and \mathbf{U}_a is the orthogonal matrix of eigenvectors;
- (iv) The quantity $\mathbf{Z} = \mathbf{U}_1 \text{diag}\left(\mathbf{U}_1^\top \mathbf{S}_2 \mathbf{U}_1\right) \mathbf{U}_1^\top$ is computed for a given split at the chosen split parameter value s ;
- (v) Over all $\binom{n}{s}$ possible choices of the split into $\mathbf{X}_{1,2}$ for the chosen value of s , the average of \mathbf{Z} is calculated to be $\bar{\mathbf{Z}}(s)$, and correspondingly the sample estimates \mathbf{S}_2 are averaged to obtain $\bar{\mathbf{S}}_2(s)$;
- (vi) The *distance* function

$$Q(s) = \|\bar{\mathbf{Z}}(s) - \bar{\mathbf{S}}_2(s)\|_{\text{F}} \quad (9)$$

(or equivalently Q^2) is minimized to find an optimal split value s^* .

The NERCOME estimator of the covariance matrix is then defined as $\hat{\Sigma}_{\text{NLS}} = \bar{\mathbf{Z}}(s^*)$. As before, the precision matrix estimator is given by its inverse, $\hat{\Psi}_{\text{NLS}} = \bar{\mathbf{Z}}(s^*)^{-1}$, and we do not include a Hartlap-like factor.

2.4 Direct linear shrinkage for the precision matrix

Instead of inverting the linear shrinkage estimator of the covariance matrix, one can apply shrinkage directly to an empirical estimate and a target for the precision matrix. Here we consider the inverse of the sample covariance matrix estimate, \mathbf{S}^{-1} , as the empirical estimate, with some suitable precision matrix target denoted by $\mathbf{\Pi}_0$ to give the direct linear shrinkage estimator of the precision matrix:

$$\mathbf{\Pi}_{\text{LS}} = \alpha \mathbf{S}^{-1} + \beta \mathbf{\Pi}_0. \quad (10)$$

Here α and β are the *mixing parameters*, and $n > d$ must be satisfied to ensure that \mathbf{S} is non-singular; in addition, the target $\mathbf{\Pi}_0$ is required to satisfy the condition $\sup_d d^{-1} \|\mathbf{\Pi}_0\|_{\text{F}}^2 \leq a$ for some constant $a > 0$.

Bodnar et al. (2016) have shown that the optimal mixing parameters can be estimated by

$$\hat{\alpha}^* = 1 - \frac{d}{n} - \frac{n^{-1} \|\mathbf{S}^{-1}\|_{\text{tr}}^2 \|\mathbf{\Pi}_0\|_{\text{F}}^2}{\|\mathbf{S}^{-1}\|_{\text{tr}}^2 \|\mathbf{\Pi}_0\|_{\text{F}}^2 - [\text{tr}(\mathbf{S}^{-1} \mathbf{\Pi}_0)]^2}, \quad (11a)$$

$$\hat{\beta}^* = \left(1 - \frac{d}{n} - \hat{\alpha}^*\right) \frac{\text{tr}(\mathbf{S}^{-1} \mathbf{\Pi}_0)}{\|\mathbf{\Pi}_0\|_{\text{F}}^2}, \quad (11b)$$

and the estimator $\mathbf{\Pi}_{\text{LS}}$ improves asymptotically as $n \rightarrow \infty$ with $d/n \rightarrow c \in (0, 1)$ for some fixed constant c .

3 APPLICATION TO POWER SPECTRUM ANALYSIS

To demonstrate the performance of the estimation methods reviewed in the previous section, we apply them to a galaxy clustering power spectrum analysis of the Baryon Oscillations Spectroscopic Survey (BOSS) Data Release 12 (DR12) catalogues (BOSS Collaboration et al. 2015; Reid et al. 2016) for the North Galactic Cap (NGC) in the redshift bin at $z = 0.38$, with the accompanying 2048 PATCHY mock catalogues (Kitaura et al. 2016) for covariance matrix estimation. The data set we use includes measurements of the clustering power spectrum monopole P_0 and quadrupole P_2 over the wavenumber range $k \in [0.01, 0.1] h \text{ Mpc}^{-1}$ in bins of width $\Delta k = 0.01 h \text{ Mpc}^{-1}$, which results in data vectors of length $d = 18$.⁴

Given the wavenumber range considered in this work, we adopt a linear redshift-space power spectrum model (Kaiser 1987) computed from Eisenstein & Hu (1998), with the fiducial cosmology taken from the Planck 2015 results (Planck Collaboration 2016). The power spectrum model includes the monopole, quadrupole and hexadecapole given by

$$P_0(k) = \left(b^2 + \frac{2}{3} b f + \frac{1}{5} f^2\right) P_m(k), \quad (12a)$$

$$P_2(k) = \left(\frac{4}{3} b f + \frac{4}{7} f^2\right) P_m(k), \quad (12b)$$

$$P_4(k) = \frac{8}{35} f^2 P_m(k), \quad (12c)$$

where P_m is the linear matter power spectrum, b is the linear bias and f is the linear growth rate. We include the wide-angle and survey window effects as matrices \mathbf{W} and \mathbf{M} respectively (Beutler & McDonald 2021),⁴ which transform the power spectrum model vector $\mathbf{P}_{\text{model}} \mapsto \mathbf{WMP}_{\text{model}}$ evaluated in the same bins as for the measurements.

To assess the performance of the different estimators with varying sample size, we have created a superset of 2040 power spectrum measurements from the 2048 mock catalogues available. This superset is divided into 85 subsets of 24 mock measurements (i.e. 85 data matrices $\mathbf{X} \in \mathbb{R}^{18 \times 24}$), or 68 subsets of 30 mock measurements each (i.e. 68 data matrices $\mathbf{X} \in \mathbb{R}^{18 \times 30}$), so that we can test covariance and precision matrix estimation with $n = 24$ and $n = 30$ sample sizes respectively.

3.1 Sample estimates

For each subset of the mock measurements, we compute a sample covariance matrix estimate \mathbf{S} using equation (1), which is then inverted

⁴ Full data set including the transformation matrices are available at fbeutler.github.io/hub/deconv_paper.

into a sample precision matrix estimate $\mathbf{\Pi}$ with the Hartlap factor γ being 0.174 for $n = 24$ and 0.344 for $n = 30$ respectively.

As a *reference* covariance matrix, we also compute the sample covariance matrix estimate \mathbf{S}_{ref} from all 2048 mock measurements, which is used to benchmark all other covariance matrix estimators. The corresponding sample precision matrix estimate $\mathbf{\Pi}_{\text{ref}}$ is used as a reference precision matrix. This has a Hartlap factor $\gamma = 0.991 \approx 1$ as $n = 2048 \gg d = 18$, and we regard it as a good proxy for the unknown true precision matrix $\mathbf{\Psi}$.

3.2 Inverted covariance shrinkage estimates

For the linear shrinkage estimator (4) of the covariance matrix, we consider two possibilities for the target matrix \mathbf{T} . The first choice, proposed by Schäfer & Strimmer (2005), is simply the diagonal of the sample covariance matrix estimate:

$$\mathbf{T}^{(1)} = \text{diag } \mathbf{S}. \quad (13)$$

In this case, only summands with $i \neq j$ contribute to the numerator and denominator of expression (8). The second choice of target, following Hamilton et al. (2006) and Pope & Szapudi (2008), is given by

$$(\mathbf{T}^{(2)})_{ij} = \frac{2}{N_i} [P_{\text{fid}}(k_i)]^2 \delta_{ij}^{(K)}, \quad (14)$$

where P_{fid} is a fiducial power spectrum model for which we set $b = 2$ and $f = 0.7$ and transform using the wide-angle and survey window matrices, and N_i is the number of modes in the bin at effective wavenumber k_i . Since $\mathbf{T}^{(2)}$ is deterministic, $\widehat{\text{Cov}}(S_{ij}, T_{ij})$ identically vanishes in equation (8).

For both choices of the target matrix, we compute the linear shrinkage estimate $\hat{\Sigma}_{\text{LS}}$ of the covariance matrix from each subset of mock measurements; this gives 85 estimates with $n = 24$ and 68 estimates with $n = 30$. The distributions of the optimal shrinkage intensity parameter $\hat{\lambda}^*$ for these two target choices are compared in Fig. 1.

We have found that the shrinkage intensity $\hat{\lambda}^*$ with target $\mathbf{T}^{(1)}$ is equal to unity for 31 out of 85 data matrices with $n = 24$ and for 21 out of 68 data matrices with $n = 30$. This indicates that in these cases, the linear shrinkage estimate in equation (4) is dominated by the target with no contribution from the sample estimate. In contrast, with target $\mathbf{T}^{(2)}$, the shrinkage intensity $\hat{\lambda}^*$ favours smaller values, which means that the target tends to contribute less to the shrinkage estimate than the sample estimate does. If the reference covariance matrix \mathbf{S}_{ref} is used as \mathbf{S} in the linear shrinkage estimator, the optimal intensity parameter is $\hat{\lambda}^* \approx 0.028$ for target $\mathbf{T}^{(1)}$ and $\hat{\lambda}^* \approx 0.002$ for target $\mathbf{T}^{(2)}$. In both cases, the linear shrinkage estimator is almost fully determined by the sample estimate of the covariance matrix. This is expected since our reference covariance matrix \mathbf{S}_{ref} is supposed to closely approximate the true covariance matrix $\mathbf{\Sigma}$.

To obtain the corresponding precision matrix estimates $\hat{\mathbf{\Psi}}_{\text{LS}}$, the aforementioned linear-shrinkage covariance matrix estimates are simply inverted.

3.3 NERCOME estimates

We follow the steps detailed in section 2.3 to compute 85 NERCOME covariance matrix estimates $\hat{\Sigma}_{\text{NLS}}$ from the data matrices $\mathbf{X} \in \mathbb{R}^{18 \times 24}$ and 68 estimates from the data matrices $\mathbf{X} \in \mathbb{R}^{18 \times 30}$. For reference, we also compute a single NERCOME estimate using all 2048 mock measurements. As before, the corresponding precision matrix estimates $\hat{\mathbf{\Psi}}_{\text{NLS}}$ are obtained by matrix inversion.

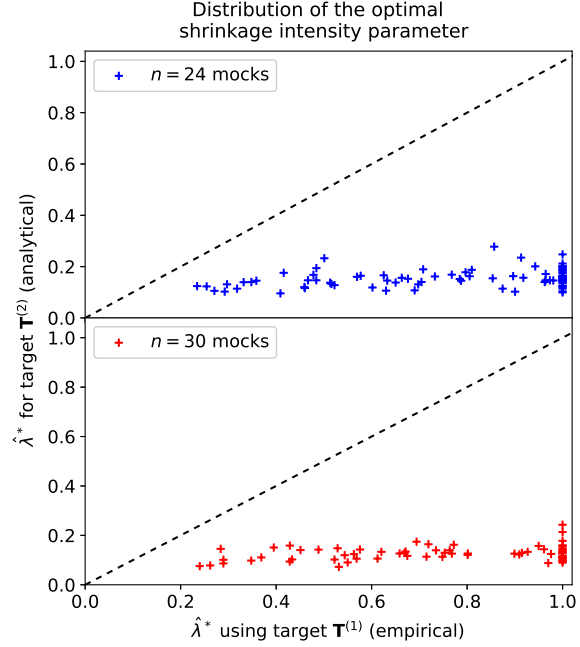


Figure 1. Distributions of the optimal shrinkage intensity $\hat{\lambda}^*$ for target matrix choices $\mathbf{T}^{(1)}$ versus $\mathbf{T}^{(2)}$. The *top panel* shows the 85 intensity parameters computed from subsets of $n = 24$ mock measurements; the *bottom panel* shows the 68 intensity parameters computed for $n = 30$. The diagonal dashed lines show the line of equality for $\hat{\lambda}^*$ between the two target choices.

A caveat here is that since $\binom{n}{s}$ can be very large for some values of s , we only randomly draw $N_{\text{draw}} = \min\{\binom{n}{s}, 1000\}$ splits of the data matrix \mathbf{X} at step (v) in section 2.3 to compute $\bar{\mathbf{Z}}(s)$ and $\bar{\mathbf{S}}_2(s)$ (Joachimi 2017).

To minimize the distance function $Q(s)$ in equation (9), we evaluate it at each point in the integer interval $s \in \llbracket 2, n-2 \rrbracket$, except when $n = 2048$, in which case we evaluate $Q(s)$ only at $s \in \{0.1n, 0.15n, 0.2n, \dots, 0.9n, 2\sqrt{n}, n - 1.5\sqrt{n}, n - 2.5\sqrt{n}\}$, as proposed by Joachimi (2017) and Lam (2016).

The distribution of the optimal split parameters s^* for all NERCOME estimates computed with $n = 24$ and $n = 30$ is shown in Fig. 2. The split-parameter distribution indicates that $s^*/n \approx 0.8$ is favoured, which is slightly different to the fixed split $s^*/n = 2/3$ found in Joachimi (2017). For reference, the split parameter for the NERCOME estimate computed using all 2048 mocks is $s^*/n = 1638/2048 \approx 0.80$.

3.4 Direct precision shrinkage estimates

Finally, for the direct linear shrinkage estimator (10) of the precision matrix, we consider two possibilities for the target matrix $\mathbf{\Pi}_0$. The first choice is the matrix consisting of eigenvalues of the inverse sample covariance matrix estimate on the diagonal, i.e.

$$(\mathbf{\Pi}_0^{(1)})_{ij} = e_i \delta_{ij}^{(K)}, \quad (15)$$

where $\{e_i\}_{i=1}^d$ are the eigenvalues of \mathbf{S}^{-1} in ascending order. The second choice is to invert the analytical covariance matrix target from equation (14),

$$\mathbf{\Pi}_0^{(2)} = (\mathbf{T}^{(2)})^{-1}. \quad (16)$$

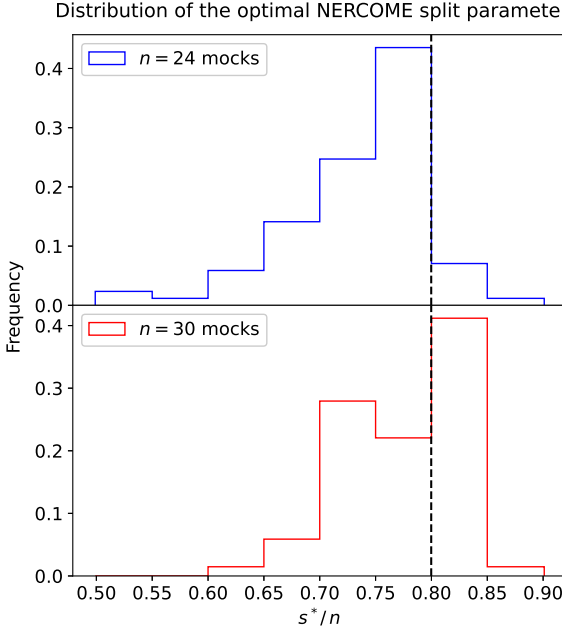


Figure 2. Normalized histogram showing the distribution of the optimal split parameter s^* that minimizes the distance function $Q(s)$ (equation 9) as a ratio s/n to the number of data realizations. The *top panel* corresponds to 85 NERCOME covariance matrix estimates computed from subsets of $n = 24$ mock measurements; the *bottom panel* corresponds to 68 estimates computed for $n = 30$. The vertical dashed line shows the optimal split parameter for $n = 2048$ mock measurements.

We then compute two linear shrinkage estimates $\boldsymbol{\Pi}_{\text{LS}}$ of the precision matrix, one per target, for each subset of mock measurements with $n = 24$ or $n = 30$ using equation (10).

The estimated optimal shrinkage mixing parameters $\hat{\alpha}^*$ and $\hat{\beta}^*$ are computed using equations (11) and shown in Fig. 3. We note that $\hat{\alpha}^*$ and $\hat{\beta}^*$ have an approximate linear relationship when $\boldsymbol{\Pi}_0^{(1)}$ is used as target. When we use $\boldsymbol{\Pi}_0^{(2)}$ as target, the linear relationship disappears. For target $\boldsymbol{\Pi}_0^{(1)}$, we have noted that $\hat{\alpha}^*$ is negative for one out of the 85 direct precision shrinkage estimates with $n = 24$, indicating that the signs of all the entries in \mathbf{S}^{-1} are flipped for this estimate. The mixing parameter $\hat{\alpha}^*$ is never negative for any other number of mock measurements n or target $\boldsymbol{\Pi}_0^{(2)}$. Moreover, it can be seen from the distribution of mixing parameters that $\hat{\alpha}^*$ becomes larger when a larger number of mock measurements is used. This indicates that the inverse sample covariance matrix estimate \mathbf{S}^{-1} has greater weight in shrinkage with larger numbers of mock measurements, as one would expect. Finally, the values of $\hat{\beta}^*$ for the target $\boldsymbol{\Pi}_0^{(2)}$ are smaller by an order of magnitude than those for the target $\boldsymbol{\Pi}_0^{(1)}$, implying that the analytical target is generally less favoured than the empirical target.

For reference, we have also listed in Table 2 the optimal shrinkage mixing parameters when \mathbf{S}_{ref} is used for the precision matrix estimate in equation (10). As expected, the $\hat{\alpha}^*$ values are close to 1 and the $\hat{\beta}^*$ values are close to 0.

4 PERFORMANCE COMPARISON

We will next compare the performance of seven types of precision matrix estimate constructed from the previous section for application

Table 2. Linear-shrinkage mixing parameters for the direct precision matrix estimate computed with $\mathbf{S} = \mathbf{S}_{\text{ref}}$ in equation (10) for different target matrices.

Target	$\hat{\alpha}^*$	$\hat{\beta}^*$
$\boldsymbol{\Pi}_0^{(1)}$ (empirical)	0.989	4.71×10^{-4}
$\boldsymbol{\Pi}_0^{(2)}$ (analytical)	0.989	1.39×10^{-5}

to the BOSS DR12 power spectrum analysis, which are listed below for clarity and completeness:

- (i) the **sample estimate** $\boldsymbol{\Pi}$ introduced in section 2.1 and computed in section 3.1;
- (ii) the inverted covariance linear-shrinkage estimate, $\hat{\boldsymbol{\Psi}}_{\text{LS}}$, introduced in section 2.2 with the empirical target $\mathbf{T}^{(1)}$ or the analytical target $\mathbf{T}^{(2)}$ defined in section 3.2 (hereafter referred to as simply the **covariance shrinkage estimate**);
- (iii) the inverted **NERCOME estimate**, $\hat{\boldsymbol{\Psi}}_{\text{NLS}}$, introduced in section 2.3 and constructed in section 3.3;
- (iv) the direct precision linear-shrinkage estimate, $\boldsymbol{\Pi}_{\text{LS}}$, introduced in section 2.4 with the empirical target $\boldsymbol{\Pi}_0^{(1)}$ or the analytical target $\boldsymbol{\Pi}_0^{(2)}$ defined in section 3.4 (hereafter referred to as simply the **precision shrinkage estimate**).

To this end, two types of performance metrics are considered: the first is based on the eigenvalue spectrum and loss function of the matrices themselves; the second is based on parameter inference, which is the ultimate objective of precision matrix estimation in cosmological likelihood analysis. The benchmark used in all comparisons is the ‘reference’ precision matrix $\boldsymbol{\Pi}_{\text{ref}}$, which we recall from section 3 is the sample estimate computed using all 2048 mock measurements and treated as a proxy for the true precision matrix $\boldsymbol{\Psi}$.

4.1 Eigenvalue spectrum and loss function

In general, since covariance and precision matrices are inversely related, smaller eigenvalues of the precision matrix correspond to larger inferred uncertainties, and the lowest eigenvalues correspond to the highest-variance principal components (eigenvectors) of the measurements. The eigenvalue spectra of the different precision matrix estimates computed from subsets of $n = 24$ mock measurements are shown in Fig. 4, and those from subsets of $n = 30$ mock measurements are shown in Fig. 5. For $n = 2048$ where all mock measurements are used in constructing the estimates (i.e. computed from the reference covariance matrix \mathbf{S}_{ref} wherever applicable), we show in Fig. 6 the relative differences between the eigenvalue spectra instead.

Overall, the agreement of the eigenvalue spectra of the estimates with that of the reference precision matrix $\boldsymbol{\Pi}_{\text{ref}}$ improves as the sample size n increases, with almost perfect agreement when $n = 2048$ as all estimates become close to the reference precision matrix itself. There are several other observations of interest:

- The sample estimates $\boldsymbol{\Pi}$ tend to lower the smallest eigenvalues, potentially leading to overestimated uncertainties;
- The covariance shrinkage estimates, $\hat{\boldsymbol{\Psi}}_{\text{LS}}$, with the target choice $\mathbf{T}^{(2)}$ tend to enlarge the largest eigenvalues, potentially leading to underestimated uncertainties. However, this does not occur for the target choice $\mathbf{T}^{(1)}$;
- The NERCOME estimates, $\hat{\boldsymbol{\Psi}}_{\text{NLS}}$, tend to decrease the largest eigenvalues, potentially leading to overestimated uncertainties;
- The precision shrinkage estimates $\boldsymbol{\Pi}_{\text{LS}}$ tend to slightly decrease the eigenvalues over the entire spectrum with the exception of the

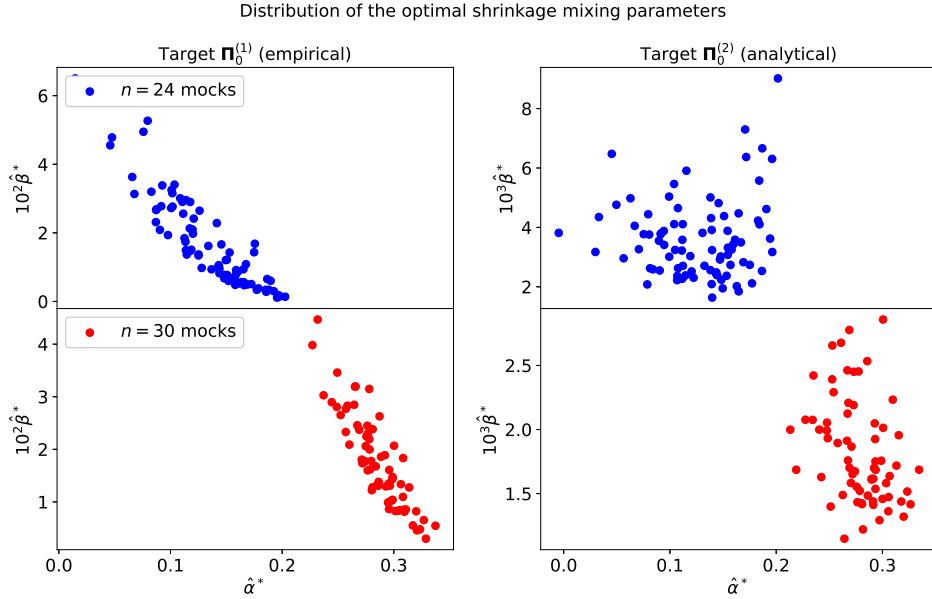


Figure 3. Distributions of the optimal linear-shrinkage mixing parameters $\hat{\alpha}^*$ and $\hat{\beta}^*$ for two choices of the target matrix Π_0 used in the direct precision matrix estimate $\hat{\Pi}_{LS}$. Each *top panel* shows the 85 mixing parameters computed for subsets of $n = 24$ mock measurements, and each *bottom panel* shows the 68 mixing parameters computed for $n = 30$. Note the different scales on the vertical axes.

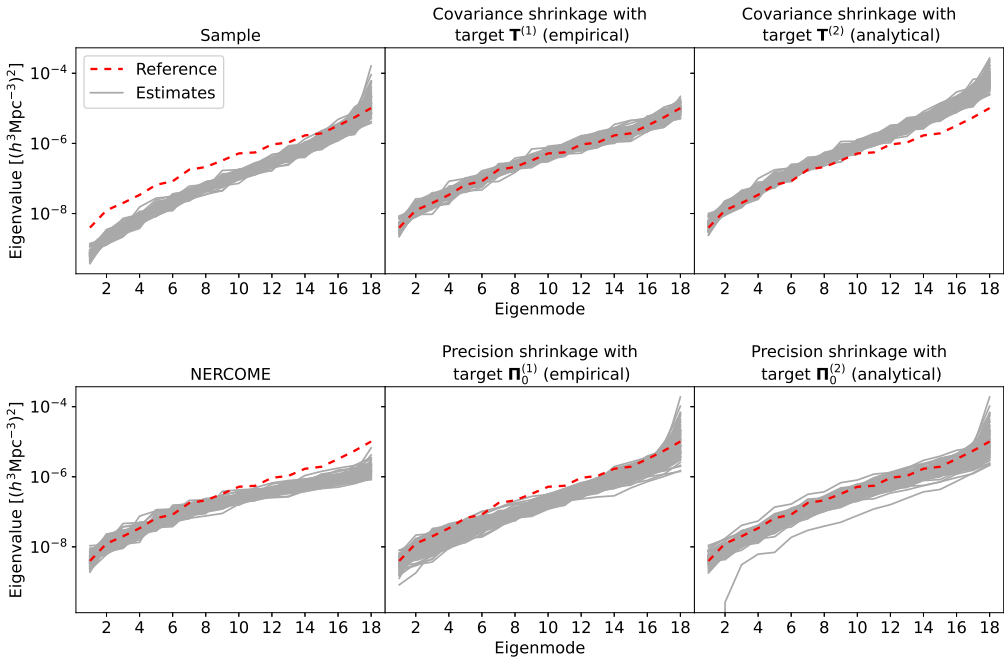


Figure 4. Eigenvalue spectra of the precision matrix estimates computed from subsets of $n = 24$ mock measurements. Each sub-figure shows the scatter of 85 spectra of one type of precision matrix estimate (with the target choice indicated where applicable), which are compared with the spectrum of the reference precision matrix Π_{ref} shown by the dashed red line.

largest eigenvalues, which are more scattered. This could potentially lead to overestimated uncertainties.

It is also observed that when we use $\Pi_0^{(2)}$ as target, one out of the 85 precision shrinkage estimates with $n = 24$ has negative eigenvalues, indicated by the grey line dropping towards zero in the bottom right plot in Fig. 4. We have noted that this precision shrinkage estimate with negative eigenvalues also has a negative $\hat{\alpha}^*$ value. We also

note that for $n = 2048$, the eigenvalues of the covariance shrinkage estimate $\hat{\Psi}_{LS}$ with target $\mathbf{T}^{(2)}$ are at a constant offset around 1% from the reference eigenvalues, as indicated by the solid orange line in Fig. 6; this is because for this particular estimate, the shrinkage intensity parameter $\lambda^* = 0.002$ is close to zero, so that it is effectively the sample estimate itself albeit without the Hartlap factor that is about 1% below unity.

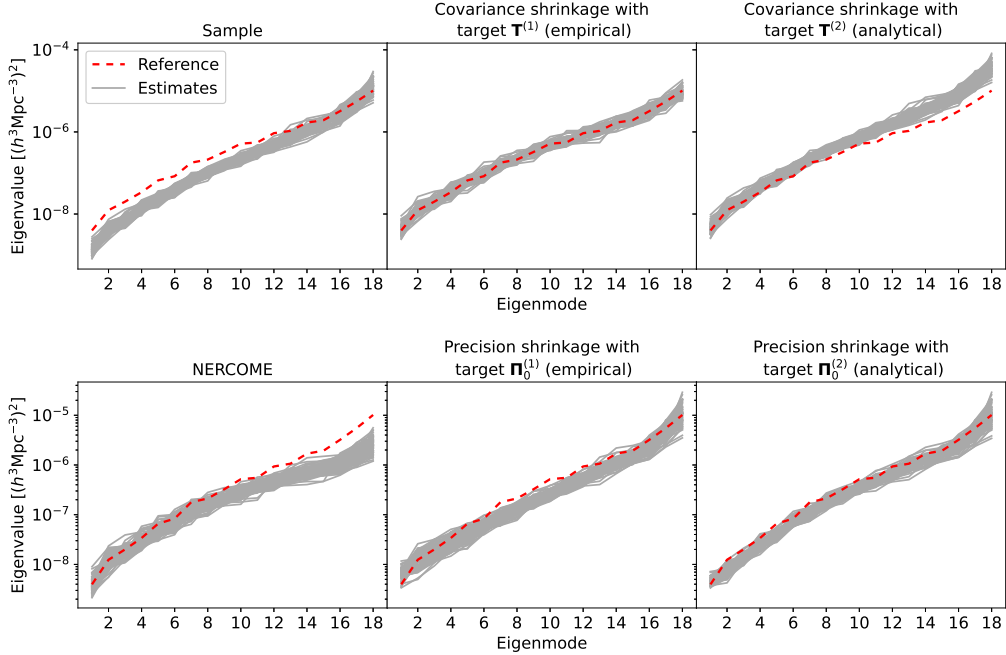


Figure 5. The same as Fig. 4, but with 68 estimates computed from subsets of $n = 30$ mock measurements in each sub-figure.

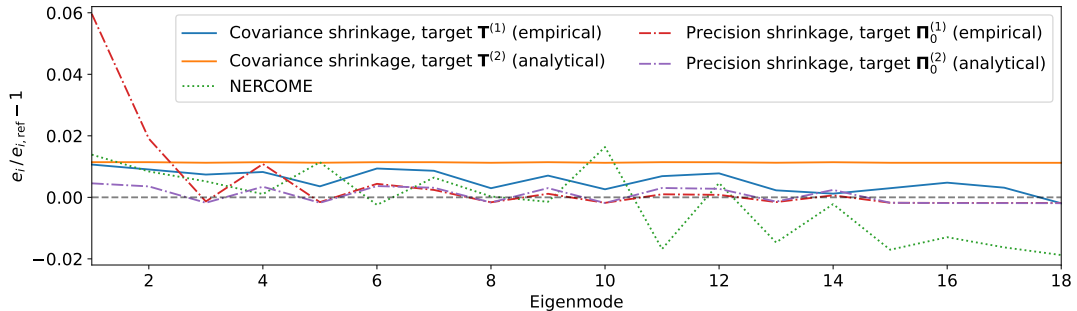


Figure 6. Relative difference, $e_i / e_{i,\text{ref}} - 1$, between the eigenvalue spectrum $\{e_i\}_{i=1}^d$ of each type of precision matrix estimate and that of the reference precision matrix, $\{e_{i,\text{ref}}\}_{i=1}^d$, all computed using all $n = 2048$ mock measurements. The dashed grey line indicates the zero reference. Note that the inverted covariance shrinkage estimate $\hat{\Psi}_{\text{LS}}$ with target $\mathbf{T}^{(2)}$ (solid orange line) is at a constant offset around 1 %, as it is very close to the sample estimate but without the Hartlap factor, which is about 1 % below unity.

To make a more direct quantitative comparison, we consider the following loss function for a generic precision matrix estimate $\hat{\Psi}$:

$$L(\hat{\Psi}; \mathbf{\Pi}_{\text{ref}}) = \left\| \hat{\Psi}^{1/2} \mathbf{\Pi}_{\text{ref}}^{-1} \hat{\Psi}^{1/2} - \mathbf{I}_d \right\|_F, \quad (17)$$

where \mathbf{I}_d is the d -dimensional identity matrix. Over all subsets of n mock measurements where $n = 24$ or 30 , we compute the median loss function and its uncertainty bounds given by the 16 % and 84 % quantiles in Table 3, with additionally a single loss function value for $n = 2048$ as there is only one precision matrix estimate of each type using all available mock measurements.

When the sample size is very close to the data vector dimension $d = 18$, e.g. $n = 24$, the covariance shrinkage estimate $\hat{\Psi}_{\text{LS}}$ with the empirical target $\mathbf{T}^{(1)}$ gives the smallest loss closely followed by the NERCOME estimate $\hat{\Psi}_{\text{NLS}}$. The precision shrinkage estimate $\mathbf{\Pi}_{\text{LS}}$ with the analytical target $\mathbf{\Pi}_0^{(2)}$ has a loss function close to that of the sample estimate $\mathbf{\Pi}$ while the other estimates result in larger losses. When $n = 30$ mock measurements are used, most shrinkage estimates have a lower loss function than the sample estimate, except the

covariance shrinkage estimate $\hat{\Psi}_{\text{LS}}$ with the analytical target $\mathbf{T}^{(2)}$ and the precision shrinkage estimate $\mathbf{\Pi}_{\text{LS}}$ with the empirical target $\mathbf{\Pi}_0^{(1)}$. When $n = 2048$, all loss function values are small. Overall, both the covariance shrinkage estimate $\hat{\Psi}_{\text{LS}}$ with the empirical target $\mathbf{T}^{(1)}$ and the NERCOME estimate $\hat{\Psi}_{\text{NLS}}$ give consistently small loss values irrespective of the sample size, whereas the shrinkage estimates with an analytical target have larger loss function values but improve rapidly with the sample size n .

4.2 Parameter inference

Since a major objective of precision matrix estimation is to obtain accurate cosmological parameter constraints in a likelihood analysis, in this section we consider the log-likelihood function (up to an

Table 3. Median of the loss function $L(\hat{\Psi})$ (equation 17) for each type of precision matrix estimate $\hat{\Psi}$ with different sample sizes n , with uncertainty bounds given by the 16 % and 84 % quantiles. Note that there is only a single loss function value when $n = 2048$, as there is only one estimate of each type computed from all available mock measurements.

Precision estimation type	$n = 24$	$n = 30$	$n = 2048$
Sample	$6.8^{+7.4}_{-2.2}$	$5.4^{+1.8}_{-1.2}$	–
Covariance shrinkage, target $\mathbf{T}^{(1)}$ (empirical)	$2.4^{+1.0}_{-0.3}$	$2.3^{+0.6}_{-0.3}$	0.051
Covariance shrinkage, target $\mathbf{T}^{(2)}$ (analytical)	$38.3^{+25.2}_{-10.5}$	$18.7^{+5.3}_{-4.3}$	0.048
NERCOME	$3.6^{+1.2}_{-0.5}$	$3.3^{+0.5}_{-0.4}$	0.049
Precision shrinkage, target $\boldsymbol{\Pi}_0^{(1)}$ (empirical)	$7.2^{+7.8}_{-2.3}$	$5.8^{+2.2}_{-1.6}$	0.064
Precision shrinkage, target $\boldsymbol{\Pi}_0^{(2)}$ (analytical)	$6.6^{+8.5}_{-3.0}$	$4.7^{+1.7}_{-1.1}$	0.013

additive constant) for each type of precision matrix estimate $\hat{\Psi}$:

$$\ln \mathcal{L}(b, f; \hat{\Psi}) = -\frac{1}{2} [\mathbf{P}_{\text{data}} - \mathbf{P}_{\text{model}}(b, f)]^\top \hat{\Psi} [\mathbf{P}_{\text{data}} - \mathbf{P}_{\text{model}}(b, f)], \quad (18)$$

where \mathbf{P}_{data} is the data vector of power spectrum monopole and quadrupole, and $\mathbf{P}_{\text{model}}$ is the model vector of power spectrum monopole, quadrupole and hexadecapole transformed by the wide-angle and survey window matrices (see section 3 for details). Note that for simplicity, we only consider varying the linear bias and growth-rate parameters b and f with all other parameters fixed to the Planck 2015 cosmology. To perform Bayesian parameter inference, we assume uniform priors $b \sim \mathcal{U}(0.5, 3.5)$ and $f \sim \mathcal{U}(0, 2)$, and sample the posterior distribution using preconditioned Monte Carlo (PMC) implemented by the pocoMC sampler (Karamanis et al. 2022b,a).

For each type of precision matrix estimate computed from $n = 24$ mock measurements, we have obtained 85 chains of the same number of posterior samples, which are then combined into a single chain of 170 000 parameter points for each estimate type; for precision matrix estimates from $n = 30$ mock measurements, 68 posterior sample chains of the same length have been generated and combined into a single chain of 136 000 parameter points for each estimate type; and for $n = 2048$ where all mock measurements are used for precision matrix estimation, a single chain of at least 2000 posterior samples has been generated for each estimate type.

In Figs. 7, 8 and 9, we show the posterior contours for the 68 % and 95 % credible regions from each type of precision matrix estimate for sample size $n = 24, 30$ and 2048 respectively, compared to the reference results obtained using the reference precision matrix $\boldsymbol{\Pi}_{\text{ref}}$. In each of these figures, we have also provided the posterior mean estimates for parameters b and f with the uncertainty bounds given by the 68 % credible interval, compared with the reference constraints $b = 1.945 \pm 0.018$ and $f = 0.617 \pm 0.043$. In principle, the uncertainty in the precision matrix estimate will increase the uncertainties of the inferred parameters; for the sample precision matrix estimate, it is possible to derive a multiplicative factor that accounts for this in the uncertainties of the maximum likelihood estimator (Dodelson & Schneider 2013), which remains a good approximation for the posterior mean estimator when the posterior distribution is close to being Gaussian (Percival et al. 2014). However, it is difficult to derive a similar factor for a generic shrinkage estimator as its probability distribution may not have an analytical form. Therefore, instead of applying this correction factor to the inferred parameter uncertainties, we rely on the fact we have combined posterior sample chains with multiple precision matrix estimates generated from equivalent subsets

of n mock measurements when $n = 24$ or 30, which should reflect the scatter in the precision matrix estimation.

When the sample size is $n = 24$, which is small and close to the data vector dimension $d = 18$, we see in Fig. 7 that the noisy sample estimate $\boldsymbol{\Pi}$ significantly worsens the parameter constraints. The covariance shrinkage estimate $\hat{\Psi}_{\text{LS}}$ with the empirical target $\mathbf{T}^{(1)}$ provides constraints much closer to the reference results, albeit very slightly over-tightened, whereas the analytical target $\mathbf{T}^{(2)}$ leads to overestimated parameter uncertainties and a few outliers out of the 85 chains sampled. This explains the protuberance in the contour boundaries for the covariance shrinkage estimate $\hat{\Psi}_{\text{LS}}$ with target choice $\mathbf{T}^{(2)}$ in Fig. 7. The NERCOME estimate $\hat{\Psi}_{\text{NLS}}$ similarly gives looser parameter constraints, and in particular there is a shift in the mean of the posterior distribution of the linear bias b , quantified at the 0.7σ level with respect to the reference results. The precision shrinkage estimate $\boldsymbol{\Pi}_{\text{LS}}$ leads to broader contours that have a different orientation to the rest, and this gives overestimated uncertainties on b , as well as slightly underestimated uncertainties on f for the analytical target $\mathbf{T}^{(2)}$.

With the sample size down to $n = 30$, improvements are seen across all types of precision matrix estimates. Again the covariance shrinkage estimate $\hat{\Psi}_{\text{LS}}$ with the empirical target $\mathbf{T}^{(1)}$ provides posteriors closest to the reference results, albeit with slightly over-tightened parameter constraints. The sample estimate $\boldsymbol{\Pi}$ has the widest parameter bounds, followed by the NERCOME estimate $\hat{\Psi}_{\text{NLS}}$ and then the other shrinkage estimates. The shift in the posterior distribution of the linear bias b produced by the NERCOME estimate $\hat{\Psi}_{\text{NLS}}$ remains, although the posterior mean is biased with respect to the reference results at a reduced level of 0.5σ . Compared with sample size $n = 24$, the difference in the orientation of the posterior contours between the precision shrinkage estimates $\boldsymbol{\Pi}_{\text{LS}}$ and the rest is lessened.

When computed from all 2048 mock measurements, all types of precision matrix estimates yield posterior constraints in close approximation to those obtained from using the reference precision matrix $\boldsymbol{\Pi}_{\text{ref}}$, as seen in Fig. 9. This indicates that given a large sample size, all estimation methods behave consistently as expected.

To quantify the differences in the posterior constraints with a varying sample size n (as shown in Figs. 7, 8 and 9), we compute the mean \hat{b} or \hat{f} and the corresponding standard deviation $\hat{\sigma}$ of the marginal posterior distributions from the combined chain for each type of precision matrix estimate; these are then compared against the reference posterior mean b_{ref} or f_{ref} and standard deviation σ_{ref} extracted from the chain obtained with the reference precision matrix, as shown in Fig. 10. It is visually clear from Fig. 10 that when n is small, the NERCOME estimate leads to a noticeable shift in the posterior mean for the linear bias b and the sample estimate

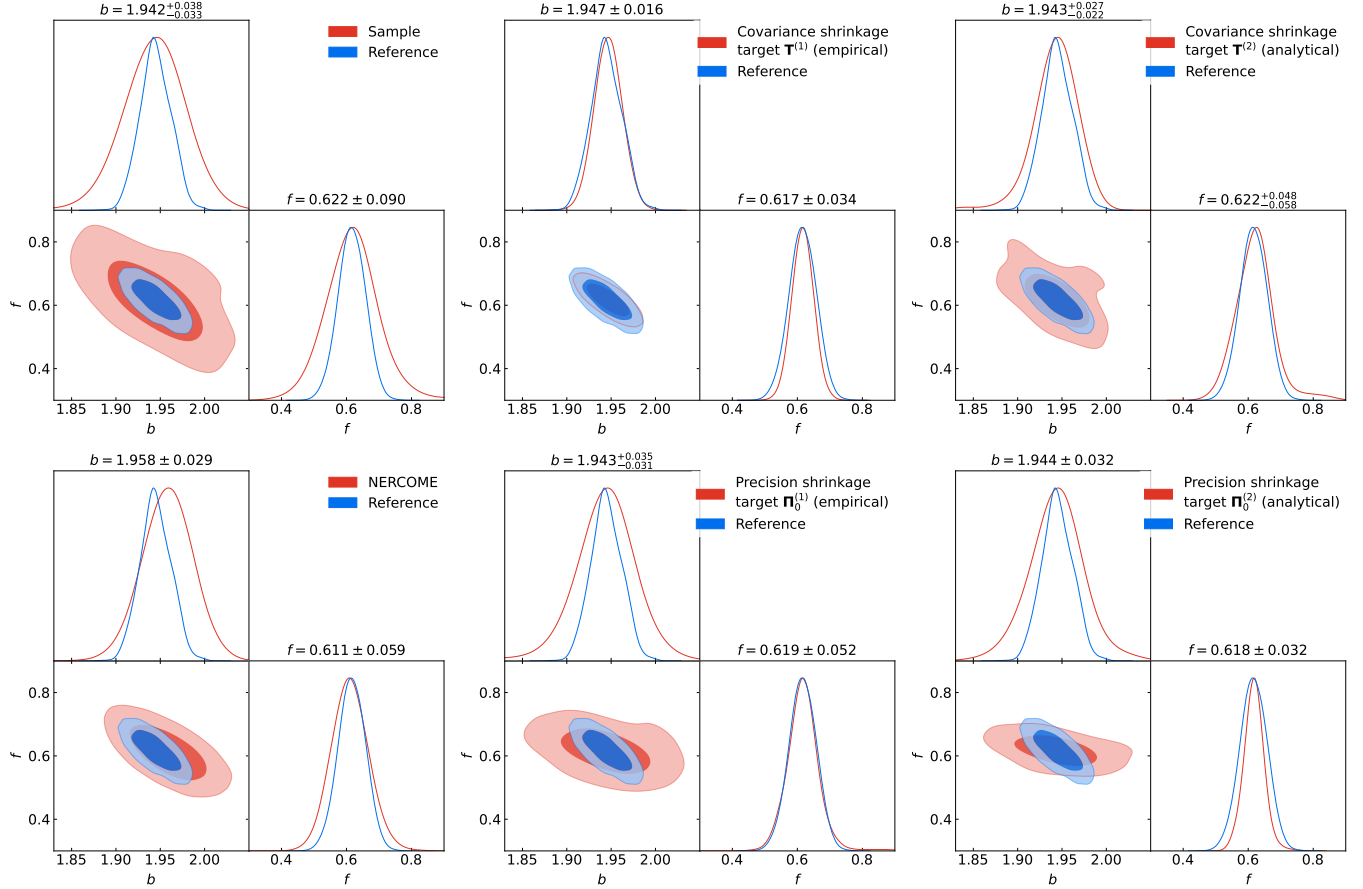


Figure 7. Posterior constraints in 68 % and 95 % credible regions on the linear bias b and growth rate f obtained using different precision matrix estimates computed from subsets of $n = 24$ mock measurements (red contours), compared to the results obtained from the reference precision matrix Π_{ref} (blue contours). The non-reference posterior mean parameter estimates are annotated above each subplot with uncertainties given by the 68 % credible interval.

leads to the most overestimated parameter uncertainties, while both the covariance shrinkage and precision shrinkage estimates produce results that are closer to the reference.

5 CONCLUSION

The determination of the covariance and precision matrices is vital to parameter inference in the era of precision cosmology. In this work, we have focused on a class of estimation methods known as shrinkage, which are used to obtain the following precision matrix estimates:

- (i) the covariance shrinkage estimate $\hat{\Psi}_{\text{LS}}$ obtained after inversion with two target choices $\mathbf{T}^{(1)}$ and $\mathbf{T}^{(2)}$, where the former is empirically based on the diagonal of the sample covariance matrix estimate and the latter is analytical (see section 3.2);
- (ii) the NERCOME (nonlinear shrinkage) estimate $\hat{\Psi}_{\text{NLS}}$ obtained after inversion (see section 3.3);
- (iii) the precision shrinkage estimate Π_{LS} with two target choices $\Pi_0^{(1)}$ and $\Pi_0^{(2)}$, where the former is empirically based on the eigenvalues of the inverted sample covariance matrix estimate and the latter is analytical (see section 3.4).

All of these shrinkage estimates, as well as the sample estimate Π , are computed for a varying sample size n and compared to the reference precision matrix Π_{ref} obtained for a large value of n .

We have applied these estimation methods to the power spectrum analysis of the BOSS DR12 data set with data vector dimension $d = 18$, in conjunction with 2048 PATCHY mock catalogues for precision matrix estimation. The performance of the different precision matrix estimates for sample size $n = 24, 30$ or 2048 is compared against the reference precision matrix constructed using all mock measurements. We have considered diagnostic metrics such as the matrix loss function and the eigenvalue spectrum; in addition, we have also performed Bayesian parameter inference of the linear bias and growth-rate parameters b and f . It has been found that:

- When the sample size is small, the covariance shrinkage estimate $\hat{\Psi}_{\text{LS}}$ with the empirical target $\mathbf{T}^{(1)}$ provides the lowest loss function values, the closest eigenvalue spectrum and the best agreement in the posterior parameter constraints compared to the reference results. With the analytical target $\mathbf{T}^{(2)}$, however, it has a higher loss function value and weaker parameter constraints.
- The NERCOME estimate $\hat{\Psi}_{\text{NLS}}$ tends to underestimate the largest precision matrix eigenvalues leading to weaker parameter constraints, which has also been demonstrated by Gouyou Beauchamps et al. (2023). It also produces a shift in the posterior mean of the bias parameter by as much as 0.7σ with respect to the reference results when $n = 24$.
- The precision shrinkage estimate Π_{LS} produces inflated parameter constraints with a slightly rotated parameter degeneracy direction

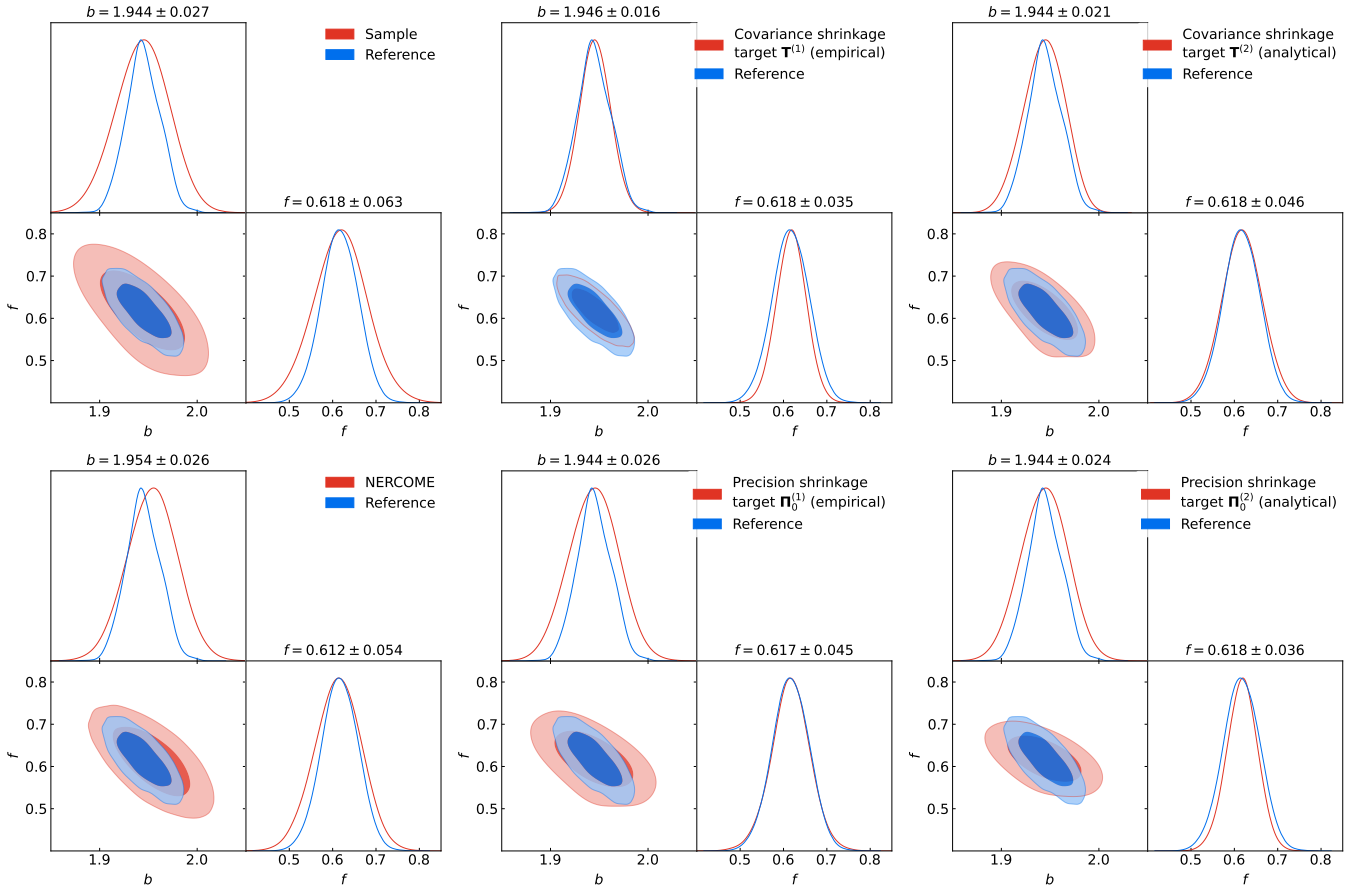


Figure 8. The same as Fig. 7 but with precision matrix estimates computed from subsets of $n = 30$ mock measurements using the different estimators discussed in the text.

for small sample size $n = 24$ or 30 , but still outperforms the sample estimate Π .

- As expected, when the sample size n is very large, all precision estimates behave similarly and give consistent posterior constraints.

Based on these configurations and results, we suggest the use of covariance shrinkage estimation of the precision matrix obtained after inversion. This serves as a useful guide for the cosmological analyses of forthcoming data releases of Stage IV galaxy surveys such as DESI and *Euclid*, where large data sets are best exploited with more performant precision matrix estimates.

Finally, we note there are many other possible choices of the shrinkage target not exhausted in this work, and their performance will depend on the precise configuration of individual cosmological analyses. In particular, although the precision shrinkage estimate has been found to give weaker parameter constraints with a rotated parameter degeneracy direction, it needs not be the case with other unexplored target choices or in a different analysis set-up. It is expected that with a target matrix that is more structurally similar to the true precision matrix Ψ (instead of the diagonal targets considered in section 3.4), e.g. an analytical target with non-linear and window function effects, these precision shrinkage estimates can be further improved. Moreover, it would offer new insight to derive correction factors similar to those in Hartlap et al. (2006) and Percival et al. (2014) to account for the stochasticity in shrinkage estimates of the precision matrix, even when they are already much less noisy than

the standard sample estimates. However, this is generally difficult since shrinkage estimates are composite quantities for which the probability distribution may be analytically intractable. We leave these considerations to future work.

ACKNOWLEDGEMENTS

The authors would like to thank Minas Karamanis for inspiration, and Uroš Seljak, Richard Grummit, Benjamin Joachimi, Julian Bautista and Taras Bodnar for helpful discussions.

This project has received funding from the European Research Council (ERC) under the European Union’s Horizon 2020 research and innovation programme (grant agreement 853291). MJL acknowledges support from the School of Physics & Astronomy at the University of Edinburgh. FB acknowledges the support of the Royal Society through a University Research Fellowship.

This work has made use of publicly available Python packages `NUMPY` (Harris et al. 2020), `SciPy` (Virtanen et al. 2020), `MATPLOTLIB` (Hunter 2007), `GETDIST` (Lewis 2019), `NBODYKIT` (Hand et al. 2018) and `pocoMC` (Karamanis et al. 2022a).

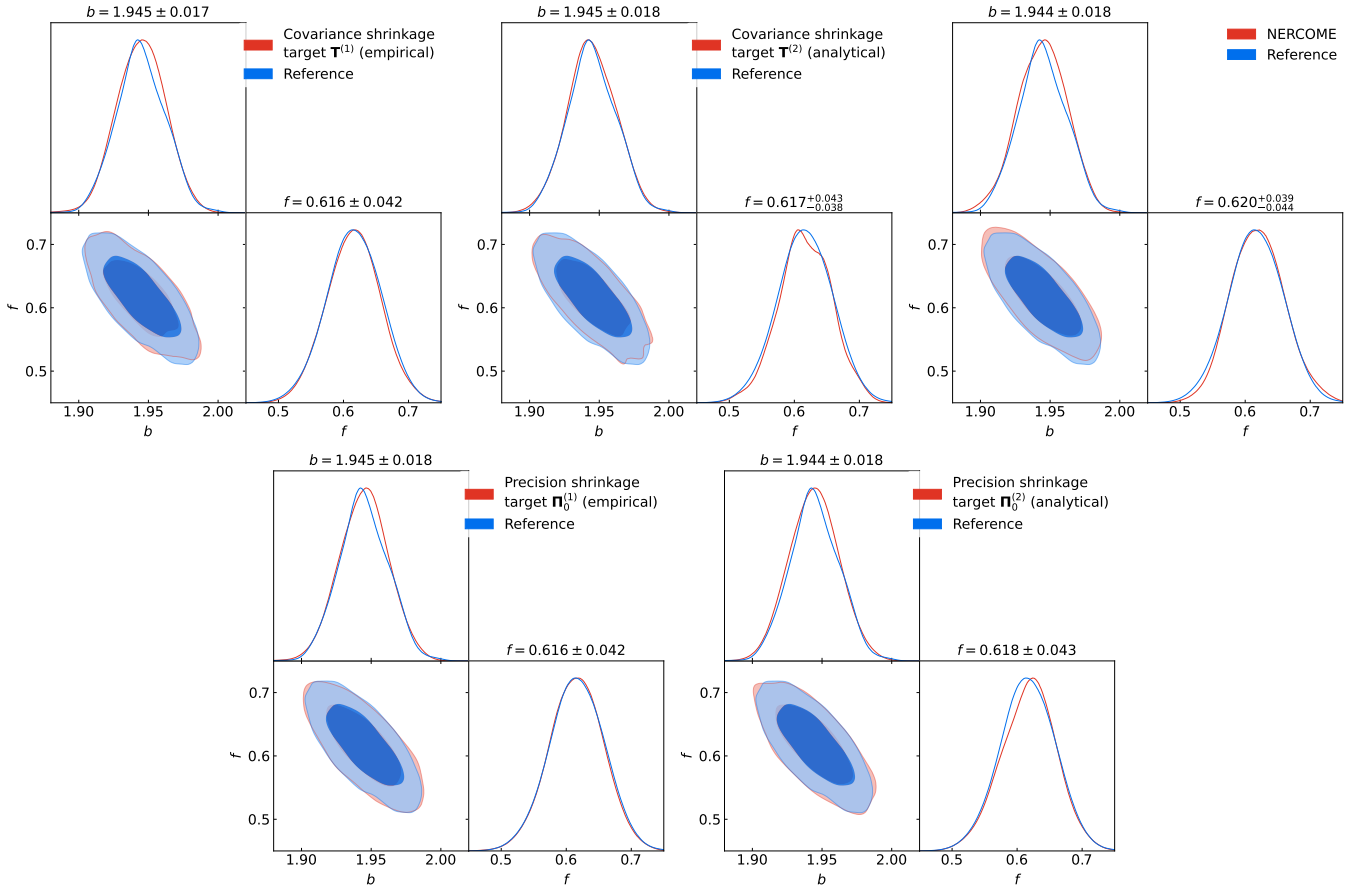


Figure 9. The same as Figs. 7 and 8 but with precision matrix estimates computed from all $n = 2048$ mock measurements using the different shrinkage estimators discussed in the text.

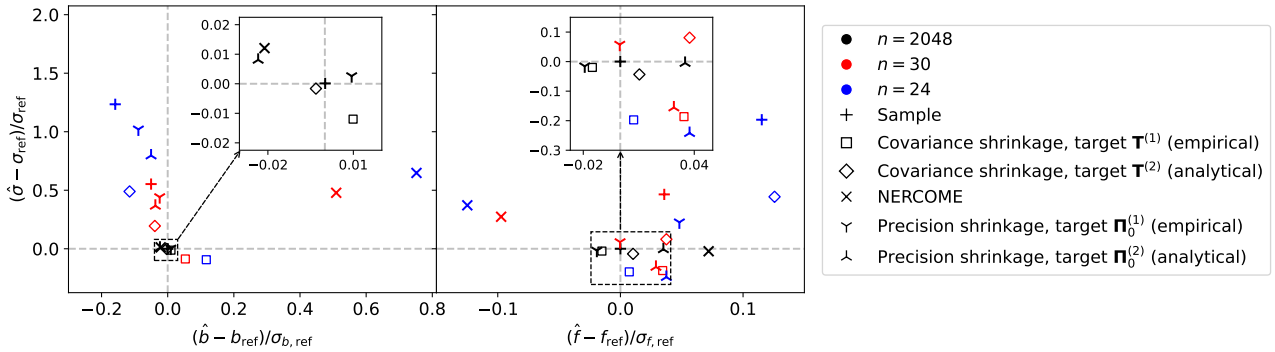


Figure 10. Relative deviations in the posterior mean and standard deviation of the linear bias b (left panel) and growth rate f (right panel) obtained from the various precision matrix estimates with a varying sample size n , compared to the reference results b_{ref} or f_{ref} and σ_{ref} obtained using the reference precision matrix. The dashed grey lines indicate the zero reference.

DATA AVAILABILITY

The data underlying this article will be shared on request to the corresponding author. The source data are available at [fbeutler.github.io/hub/deconv_paper](https://github.com/fbeutler/github.io/hub/deconv_paper), and any generated data, including the code used to derive further data, are available at github.com/marnixlooijmans/shrinkage-estimation-paper.

REFERENCES

- Abadir K. M., Distaso W., Žikeš F., 2014, *J. Econom.*, 181, 165
- d'Amico G., Gleyzes J., Kokron N., Markovic K., Senatore L., Zhang P., Beutler F., Gil-Marin H., 2020, *J. Cosmology Astropart. Phys.*, 2020, 005
- BOSS Collaboration et al., 2015, *ApJS*, 219, 12
- Beutler F., McDonald P., 2021, *J. Cosmology Astropart. Phys.*, 2021, 031
- Bodnar T., Gupta A. K., Parolya N., 2016, *J. Multivar. Anal.*, 146, 223
- DESI Collaboration 2023, preprint ([arXiv:2306.06308](https://arxiv.org/abs/2306.06308))
- DESI Collaboration 2024, *AJ*, 167, 62
- Dodelson S., Schneider M. D., 2013, *Phys. Rev. D*, 88, 063537

- Eisenstein D. J., Hu W., 1998, *ApJ*, 496, 605
 Escoffier S. et al., 2016, preprint ([arXiv:1606.00233](https://arxiv.org/abs/1606.00233))
 Friedrich O., Seitz S., Eifler T. F., Gruen D., 2015, *MNRAS*, 456, 2662
 Gouyou Beauchamps S., Baratta P., Escoffier S., Gillard W., Bel J., Bautista J., Carbone C., 2023, preprint ([arXiv:1110.3193](https://arxiv.org/abs/1110.3193))
 Grieb J. N., Sánchez A. G., Salazar-Albornoz S., Vecchia C. D., 2016, *MNRAS*, 457, 1577
 Hamilton A. J., Rimes C. D., Scoccimarro R., 2006, *MNRAS*, 371, 1188
 Hand N., Feng Y., Beutler F., Li Y., Modi C., Seljak U., Slepian Z., 2018, *AJ*, 156, 160
 Harris C. R. et al., 2020, *Nature*, 585, 357
 Hartlap J., Simon P., Schneider P., 2006, *A&A*, 464, 399
 Hunter J. D., 2007, *Comput. Sci. Eng.*, 9, 90
 Joachimi B., 2017, *MNRAS*, 466, L83
 Kaiser N., 1987, *MNRAS*, 227, 1
 Karamanis M., Nabergoj D., Beutler F., Peacock J. A., Seljak U., 2022a, *J. Open Source Softw.*, 7, 4634
 Karamanis M., Beutler F., Peacock J. A., Nabergoj D., Seljak U., 2022b, *MNRAS*, 516, 1644
 Kitaura F. S. et al., 2016, *MNRAS*, 456, 4156
 Lam C., 2016, *Ann. Stat.*, 44, 928
 Laureijs R. et al., 2011, preprint ([arXiv:1110.3193](https://arxiv.org/abs/1110.3193))
 Ledoit O., Wolf M., 2003, *J. Empir. Financ.*, 10, 603
 Ledoit O., Wolf M., 2004, *Journal of Multivariate Analysis*, 88, 365
 Ledoit O., Wolf M., 2012, *Ann. Stat.*, 40, 1024
 Lewis A., 2019, preprint ([arXiv:1910.13970](https://arxiv.org/abs/1910.13970))
 Li Y., Singh S., Yu B., Feng Y., Seljak U., 2019, *J. Cosmology Astropart. Phys.*, 2019, 016–016
 Mohammad F. G., Percival W. J., 2022, *MNRAS*, 514, 1289
 O’Connell R., Eisenstein D. J., 2019, *MNRAS*, 487, 2701–2717
 Percival W. J. et al., 2014, *MNRAS*, 439, 2531
 Perko A., Senatore L., Jennings E., Wechsler R. H., 2016, preprint ([arXiv:1610.09321](https://arxiv.org/abs/1610.09321))
 Philcox O. H. E., Eisenstein D. J., O’Connell R., Wiegand A., 2019, *MNRAS*, 491, 3290–3317
 Planck Collaboration 2016, *A&A*, 594, A13
 Pope A. C., Szapudi I., 2008, *MNRAS*, 389, 766
 Reid B. et al., 2016, *MNRAS*, 455, 1553
 Schäfer J., Strimmer K., 2005, *Stat. Appl. Genet. Mol. Biol.*, 4
 Sellentin E., Heavens A. F., 2016, *MNRAS*, 456, L132
 Semenaitė A. et al., 2022, *MNRAS*, 512, 5657
 Sugiyama N. S., Saito S., Beutler F., Seo H. J., 2020, *MNRAS*, 497, 1684
 Taylor A., Joachimi B., 2014, *MNRAS*, 442, 2728
 Taylor A., Joachimi B., Kitching T., 2013, *MNRAS*, 432, 1928
 de la Torre S. et al., 2013, *A&A*, 557, A54
 Virtanen P. et al., 2020, *Nature Methods*, 17, 261
 Wadekar D., Scoccimarro R., 2020, *Phys. Rev. D*, 102, 123517
 Wadekar D., Ivanov M. M., Scoccimarro R., 2020, *Phys. Rev. D*, 102, 123521

This paper has been typeset from a Te_X/L_AT_EX file prepared by the author.